https://doi.org/10.5194/egusphere-2025-3219
Preprint. Discussion started: 25 August 2025

Key Role of Nitrogen-containing Oxygenated Organic Molecules (OOMs) in SOA Formation Evidenced by OH/NO_3-induced Terpinolene Oxidation

Hongjin Wu[1], Juan Dang[1*], Xiaomeng Zhang[1], Weichen Yang[1], Shuai Tian[2], Shibo Zhang[1*], Qingzhu Zhang[1], Wenxing Wang[1]

1. *Environment Research Institute, Shandong University, Qingdao 266237, China*
2. *Department of Cardiology, The Eighth Affiliated Hospital, Sun Yat-sen University, Shenzhen, Guangdong 518033, China*

Keywords: Oxygenated organic molecules; Terpinolene; SOA formation; Atmospheric oxidation; Atmospheric chemical model

*Corresponding author.
E-mail address: zhangshibo@sdu.edu.cn (Shibo Zhang); dangj@sdu.edu.cn (Juan Dang)

https://doi.org/10.5194/egusphere-2025-3219
Preprint. Discussion started: 25 August 2025

Abstract

Oxygenated organic molecules (OOMs), generated from the oxidation of various biogenic volatile organics with diverse yields, are a great contributor to SOA formation. Terpinolene is an isomeride of limonene, with an even higher SOA yield. Herein we investigated the elaborate oxidation mechanism of terpinolene by OH and NO_3, elucidating the new formation mechanism of OOMs and their yield profiles based on the newly-built zero-dimensional chemical model under three typical atmospheric conditions. For terpinolene oxidation by OH, H shift imposes restrictions on continuous autoxidation, instead by the reactions with HO_2/NO/NO_2 resulting in chain termination. For the reaction of terpinolene with NO_3, the transfer of the radical center via bond breaking, triggering a new round of autoxidation, is newly found to be pivotal in the formation of nitrogen-containing OOMs with high yields. The effective saturation concentration (C^*) of nitrogen-containing OOMs is mostly lower than the OOMs formed by OH oxidation, more easily distributed into particle phase. The estimated C^* of the generated OOMs are distinctly varied among OOM isomers, which emphasizes the necessity of determining their molecular structures, peculiarly the number of rings. The comparative analysis of OH-initiated (daytime) and NO_3-driven (nocturnal) terpinolene oxidation mechanism, highlighted the formation of nitrogen-containing OOMs, would be conducive to molecular structures identification of OOMs in atmospheric monitoring and atmospheric chemical model refinement.

https://doi.org/10.5194/egusphere-2025-3219
Preprint. Discussion started: 25 August 2025

1 Introduction

In the atmosphere, the multi-generation oxidation reactions of biogenic or anthropogenic volatile organics lead to the formation of oxygenated organic molecules (OOMs) and highly oxygenated organic molecules (HOMs), which are important contributors to secondary organic aerosol (SOA) formation. Given the low volatility, HOMs and OOMs could participate in the nucleation of new particles or condense on the particulate matter to enhance SOA formation. It is well known that SOA has a significant impact on air quality and climate change through scattering and absorbing solar radiation, and serving as cloud condensation nuclei (Shen et al., 2022). Hence, clarifying the formation mechanism of OOMs/HOMs is a vital issue for atmospheric chemistry.

Numerous C10OOMs are generated from monoterpenes ($C_{10}H_{16}$), which is one of the most abundant OOM species in the forests (Bianchi et al., 2017). For instance, the percentage of monoterpene-derived OOMs can be up to 76% in a forested area of southern boreal Finland (Qiao et al., 2023). In urbanized areas of eastern China, the increase in vegetational cover generates a mix of anthropogenic and biological emissions which contribute to SOA formation (Wang et al., 2020), suggesting that monoterpene OOMs are of concern in urban areas, not only in forested areas (Huang et al., 2016). Concretely, monoterpene OOMs have been detected in recent urban atmospheric observations, approximately 30% of the particulate generation below 10 nm is attributed to monoterpene OOMs in Nanjing (Huang et al., 2016). Measurements in forested areas revealed that monoterpene oxidation products played a dominant role in driving new particle growth (Mohr et al., 2019; Huang et al., 2016), while the atmospheric oxidation mechanisms of monoterpenes to form OOMs have not been fully elucidated.

Previous research mainly focused on the molecular composition (Liu et al., 2021; Nie et al., 2022; Guo et al., 2022), the information on the molecular structure is limited which hindered a well-grounded understanding of the atmospheric fate of OOMs (Garmash et al., 2020; Kurtén et al., 2017; Bianchi et al., 2019). For instance, when tried to identify the OOMs detected from the field observation, 151 chemical formulas could be categorized as monoterpenes or aromatic hydrocarbons, which would lead to the deviations in OOMs detection and SOA formation estimation (Qiao et al., 2023). In addition to forming new particles, the relative contribution of

https://doi.org/10.5194/egusphere-2025-3219
Preprint. Discussion started: 25 August 2025

OOMs to SOA formation is governed by their net condensation potential, primarily determined by vapor concentrations and volatility (Wang et al., 2022). Generally, the higher the oxygen content of OOMs, the lower their volatility. Given the lack of pure standards, especially for complex multifunctional oxidation products such as OOMs, the measured saturated vapor pressure data are extremely limited. Therefore, the field observations and laboratory studies have employed a two-dimensional volatility basis set (2D-VBS) classification framework to identify the key SOA-contributing components by combining the effective saturation concentration (C^*) and the oxidation state of the oxidation products. In addition, the volatility of the organics with the same molecular formula could vary dramatically due to the structural difference in the functional groups and hydrogen bond (Bianchi et al., 2019; Vasudevan-Geetha et al., 2024). Currently, the molecular structures of OOMs have not been adequately determined in the field measurements and laboratory investigations, the assessment of their volatility deserves further research.

The atmospheric models typically only consider the representative monoterpene (such as α-pinene), but the SOA yields of different monoterpenes vary widely even with analogous structure (Friedman and Farmer, 2018; Draper et al., 2015; Fry et al., 2014; Kurtén et al., 2017; Vasudevan-Geetha et al., 2024). In this work, terpinolene is selected as model compound due to its high SOA yield. As a kind of cyclic diolefins with an endocyclic and an exocyclic double bond(Griffin et al., 1999), terpinolene has an atmospheric lifetime of 2 hours or less (Corchnoy and Atkinson, 1990). The estimated annual emission of terpinolene is roughly 1.3 Tg yr^{-1} (Reissell et al., 1999; Guenther et al., 2012), which is emitted by deciduous tree species such as Sophora japonica and Ginkgo biloba, as well as medicinal plants like Amomum tsaoko seeds (Lindwall et al., 2015). The previous studies have investigated the reaction of terpinolene with O_3 by experimental or theoretical methods (Atkinson et al., 1992; Orzechowska, 2003; Herrmann et al., 2010; Aschmann et al., 2002; Kim, 2016; Lee et al., 2006; Shu and Atkinson, 1994; Atkinson et al., 1990; Witter et al., 2002; Luo et al., 1996). For the reaction of OH with terpinolene, the rate constant is 2.25×10^{-10} $cm^3molecule^{-1}s^{-1}$ (Corchnoy and Atkinson, 1990; Griffin et al., 1999), and the yields of two main products, acetone (32~39%) and 4-methyl-3-cyclohexen-l-one (~26%), have been determined (Orlando et al., 2000; Hakola et al., 1994; Reissell et al., 1999). Notably, the OH-initiated oxidation of terpinolene demonstrates a

https://doi.org/10.5194/egusphere-2025-3219
Preprint. Discussion started: 25 August 2025

distinctly higher SOA yield (33% at 5.7 days aging time) compared to α-pinene and limonene (Friedman and Farmer, 2018; Surratt et al., 2008). Except for the daytime atmospheric oxidation induced by OH and O_3, NO_3-initiated reactions have been identified as a pivotal nocturnal pathway for terpinolene, with a rate constant of (6.0±3.8) × 10^{-11} $cm^3molecule^{-1}s^{-1}$ (Fouqueau et al., 2022). Experimental studies have identified first- and second-generation oxidation products (such as $C_{10}H_{16}O_3$ and $C_8H_{17}N_2O_4$) and proposed that the oxidation mechanism of terpinolene initiated by NO_3 is dominated by NO_3 addition (Fouqueau et al., 2022), with the SOA yield of up to 60% (Corchnoy and Atkinson, 1990; Fouqueau et al., 2022; Stewart et al., 2013; Griffin et al., 1999; Martínez et al., 1999). As an important precursor for SOA formation, the OOMs formation mechanisms derived from terpinolene remain unclear, which is critical for deepening the understanding of SOA formation and refining the atmospheric models.

In this study, we combined oxidation mechanism investigation and newly-built kinetic modeling to systematically elaborate OOMs formation from terpinolene oxidation initiated by OH and NO_3 radical, illustrating the yield profiles of OOMs and other products. Additionally, we utilized the functional group contribution method and the molecular formula parameterization method to estimate the saturated vapor pressures of the OOMs to evaluate their contribution to NPF and SOA formation. The comparative investigation of OH-initiated and NO_3-driven oxidation mechanisms of terpinolene, especially for the formation of OOMs, is expected to fill the gap between ambient monitoring of SOA and atmospheric model forecast.

2 Methods

2.1 Electronic structure and energy calculations

All the quantum chemical calculations were performed utilizing Gaussian 16 software. Conformational optimizations for the reactants, intermediates, transition states, and products were all carried out at the M06-2X/6-31+G(d, p) computational level. Intrinsic reaction coordinate (IRC) was conducted to ensure that the transition states were related to the matching reactants and products at the same computational level. The single point energies were calculated at M06-2X/6-311++G(3df,3pd) level enhanced the accuracy of energies. The distribution of average local ionization energies (ALIE) was plotted using Multiwfn (Lu and Chen, 2012) combined with VMD (Humphrey et al., 1996) for terpinolene to specify its

https://doi.org/10.5194/egusphere-2025-3219
Preprint. Discussion started: 25 August 2025

electron-rich sites.

2.2 Kinetics calculations

The rate constants of the reactions are calculated by transition state theory, with the tunneling effect corrected by the Wigner method. The pseudo-first-order rate constants for the bimolecular reactions were derived from the rate constants of RO_2 radicals with HO_2/NO/NO_2 and the concentrations of the reactants under the atmospheric conditions of the polluted, forested, and remote area. The reaction rate constants were all calculated at 298 K, 1 atm. Using MATLAB, the zero-dimensional chemical models are established based on the oxidation mechanism and kinetics of the alkyl radicals (Ter-R•) produced by the reactions of terpinolene with OH and NO_3 radical.

2.3 Vapor prediction

The functional group contribution method (SIMPOL.1) was used to predict the saturation vapor pressures based on the molecular structure and functional groups of the OOMs (Pankow and Asher, 2008). In addition, the molecular formula parameterization method is also employed to calculate the effective saturation concentration(C^*) of the OOMs, which was optimized by Mohr et al. (Mohr et al., 2019) based on the HOMs dataset (Tröstl et al., 2016), the details of these methods are provided in the Supporting Information S1.

3 Results and discussion

For the clarity of the molecular structure and reaction pathways, the carbon atoms of terpinolene were labeled as shown in Fig. S1. Analysis of the ALIE distribution revealed that the two double bonds exhibit the lowest ALIE values, indicating their highest reactivity as the primary reactive sites.

3.1 Initial reactions of Terpinolene with OH/NO_3 radical

https://doi.org/10.5194/egusphere-2025-3219
Preprint. Discussion started: 25 August 2025

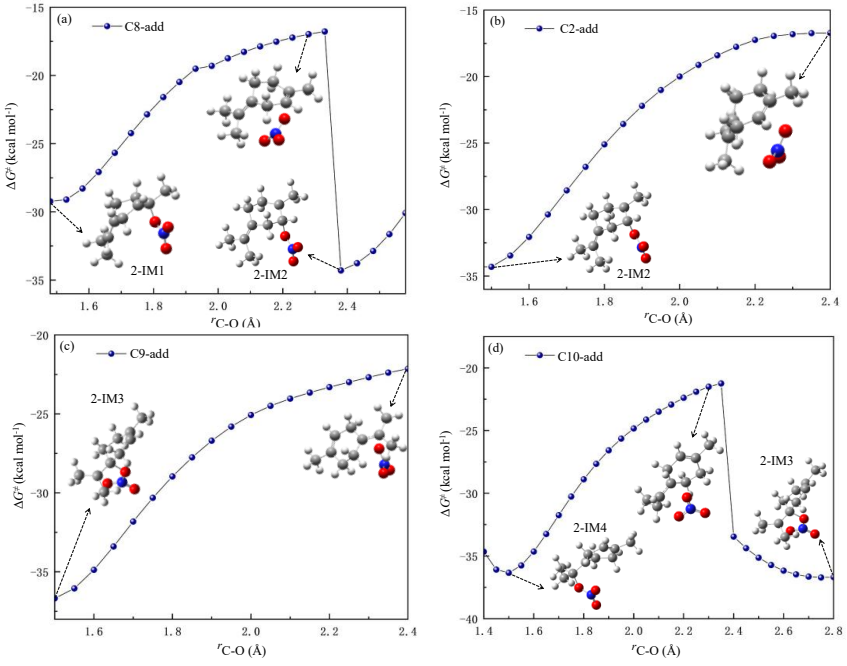

Figure 1. Scanned potential energy surfaces for NO_3 radical addition reactions (unit in kcal mol^{-1})

The initial reactions of terpinolene with OH radical primarily proceed via two mechanisms (Fig. S2), i.e., OH radical addition to two nonconjugated double bonds and H-abstraction by OH radical. All the addition reactions are exergonic and thermodynamically feasible in the atmosphere with the energy barriers of 1.9 ~ 4.7 kcal mol^{-1}, leading to the formation of OH-terpinolene adducts. Analogous to addition reactions, the H-abstraction processes are all exergonic with small free energy barriers (4.9 ~ 9.0 kcal/mol), yielding seven alkyl radicals. The OH addition is dominant over the H-abstraction reaction pathway, which is consistent with the previous laboratory studies (Arey et al., 1990; Orlando et al., 2000; Reissell et al., 1999).

Similar to OH radical, NO_3 radical addition and H-atom abstraction from the carbon chain by NO_3 radical are the initial reaction pathways of terpinolene with NO_3. Notably, NO_3 radical migration is observed in NO_3 addition processes, as shown in the potential energy surface scans at the M06-2X/6-311++G(3df, 3pd) computational level in Fig. 1 (a) and (d), the addition of NO_3 radical to C8 and C10 site produce 2-IM1 and 2-IM4, respectively, which then undergo NO_3 migration to generate 2-IM2 and 2-IM3, overcoming low energy barriers. According to

https://doi.org/10.5194/egusphere-2025-3219
Preprint. Discussion started: 25 August 2025

Fig. 3 (b) and (c), the energy increases with the gradual rising distance of the C-O bond without a saddle point. Therefore, these two addition reactions are considered as barrierless processes. Regarding the H abstraction by NO_3 radical, it can be seen from Fig. S3 that the abstraction reactions are all exothermic (-0.7 ~ -27.8 kcal mol^{-1}), crossing the energy barriers of 1.2 ~ 16.4 kcal mol^{-1} to produce seven different radical intermediates.

3.2 The oxidation of alkyl radicals (Ter-R•) initiated by OH/NO_3 radical

3.2.1 The oxidation of OH-Terpinolene-R• (1-IM4 and 1-IM7)

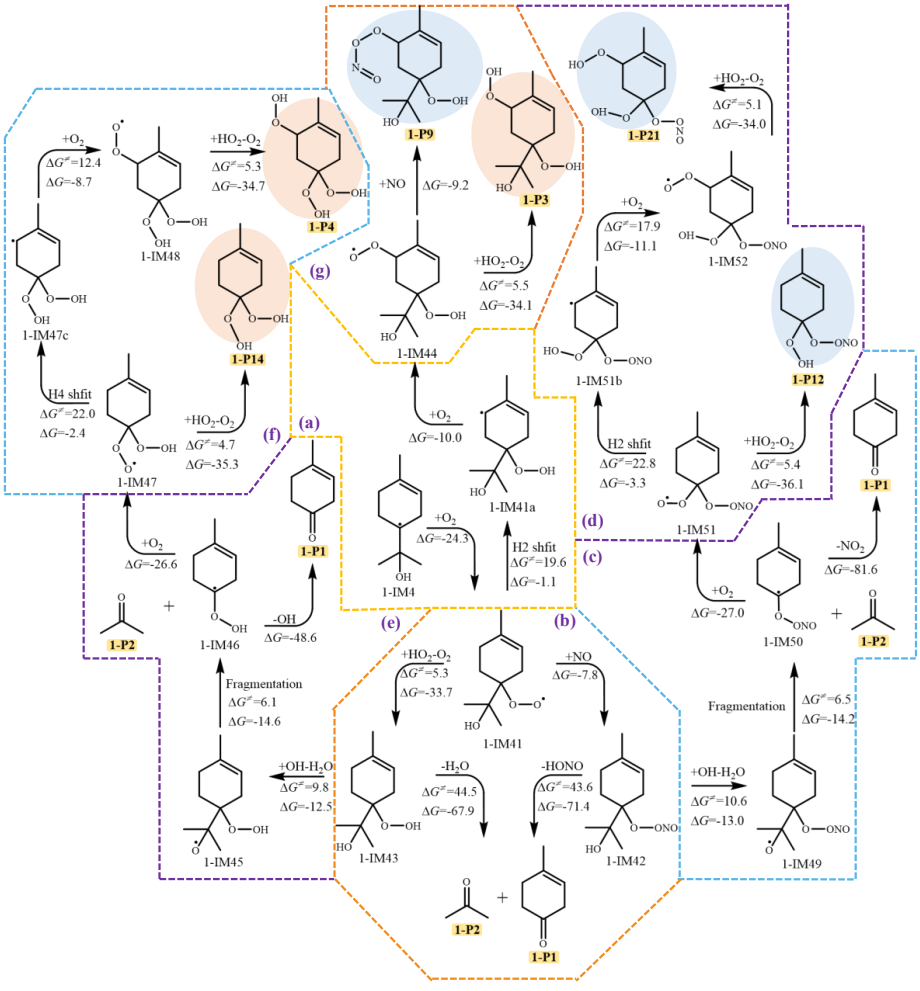

Figure 2. The subsequent reactions of OH-Ter-R• (1-IM4) (unit in kcal mol^{-1}, nitrogen-containing OOMs marked in light blue, nonnitrogenous OOMs marked in lightsalmon)

https://doi.org/10.5194/egusphere-2025-3219
Preprint. Discussion started: 25 August 2025

The alkyl radicals (1-IM4 and 1-IM7) were selected for in-depth study of atmospheric oxidation mechanism, which are the dominant intermediates formed from OH addition and H-abstraction reactions, respectively. Similar to other C-centered radicals, the reaction with O_2 is the main pathway of 1-IM4 (Peeters et al., 2014). As shown in Fig. 2, 1-IM4 undergoes a rapid barrierless association reaction with O_2, which is exoergic by 24.3 kcal mol^{-1}, leading to the generation of 1-IM41. Three competitive reaction pathways of 1-IM41 are considered: conjugation reaction with NO to generate 1-IM42 under high NO_x condition, reaction with HO_2 to form the intermediate 1-IM43 under the atmospheric condition of low NOx, and the isomerization reactions including the cyclization and hydrogen shift. The aforementioned reactions of 1-IM42 and 1-IM43 can both generate 1-P1 and 1-P2, which have been detected in laboratory studies of the reaction of terpinolene with OH radical (Hakola et al., 1994). Unlike the formation mechanism of 1-P2 in the previous experimental research, which proposed that the intermediate generated by the association with NO could directly lead to the formation of 1-P2 and 1-P1 through the removal of NO_2 (Fig. S4) (Orlando et al., 2000; Reissell et al., 1999), we found that HONO is eliminated from 1-IM42 other than NO_2, with a relatively high energy barrier. In addition, 1-IM42 can also undergo H-atom abstraction by OH and the C-C bond cleavage to generate 1-IM50, followed by the elimination of NO_2 yielding 1-P1 and 1-P2. Similarly,1-IM43 can either undergo the removal of H_2O or H-atom abstraction followed by the fragmentation of the C-C and O-O bond, leading to the formation of the new C7 alkyl radicals (1-IM46), 1-P1 and 1-P2, of which, by comparing the energy barriers, the latter pathway is easier to occur under atmospheric conditions. As depicted in Fig. 2(d),1-IM50 can further react with O_2 to generate the peroxyl radical 1-IM51, which then reacts with HO_2 to generate 1-P12 or triggers a new round of autoxidation, with H2 shift (1,5 H shift) as the dominant reaction, leading to the formation of 1-P21. Analogously, 1-IM46 can undergo O_2 addition to generate a peroxyl radical 1-IM47, ultimately resulting in the generation of 1-P4 and 1-P14. According to the traditional autoxidation mechanism (Fig. 2(a)), 1-IM41 undergoes H2 shift (1,5 H shift) to form 1-IM41a with an energy barrier of 19.6 kcal mol^{-1}, which further reacts with O_2 to produce a new peroxyl radical 1-IM44. Whereas, the subsequent oxidation of 1-IM44 is restricted due to the high energy barriers of the H shift and cyclization reactions (Fig. S6), which cannot occur spontaneously under atmospheric conditions. Therefore, 1-IM44 can

https://doi.org/10.5194/egusphere-2025-3219
Preprint. Discussion started: 25 August 2025

only react with HO_2 to form 1-P3 or react with NO to produce a nitrogenous OOM 1-P9, which have been identified as the major monoterpene-derived C10OOMs in the field observations (Luo et al., 2023; Guo et al., 2022; Zheng et al., 2023). The presence of the endocyclic double bond enables 1-IM41 to undergo cyclization to generate 1-IM41f and 1-IM41g, which are thermodynamically unfavorable under atmospheric conditions (Fig. S5).

The subsequent reaction pathway of 1-IM7 is initiated with O_2 addition to form the peroxyl radical 1-IM71, which further reacts with HO_2 to generate 1-IM74, followed by the hydrogen abstraction by OH radical and OH elimination to yield 1-P7 (Fig. 3(b)). 1-IM71 can also react with NO, consecutively proceeding with NO_2 elimination and the binding with O_2 to produce the peroxyl radical 1-IM78. As shown in Fig. 3(c), 1-IM78 can sequentially react with HO_2/NO to generate 1-P8 and 1-P11, respectively. In addition, 1-IM78 can also undergo H4 shift (1,6 H shift) to form 1-IM78d, which subsequently reacts with O_2 to generate a new peroxyl radical 1-IM79, eventually leading to the production of 1-P13, which has been detected in the field observation and the laboratory studies of limonene oxidation by OH (Luo et al., 2023; Zheng et al., 2023). Furthermore, the peroxyl radical 1-IM79 can react with NO/NO_2 to produce nitrogen-containing OOMs 1-P15 and 1-P16. Additionally, the peroxyl radical 1-IM71 undergoes the H4 shift (1,5 H shift) and the association with O_2 to produce a new peroxyl radical 1-IM72, which can further react with HO_2 to generate the OOM 1-P5, or react with NO/NO_2 to form 1-P17 and 1-P18, respectively (Fig. 3(e)). Analogously, Fig. 3(f) indicates that the peroxyl radical 1-IM72 can undergo a subsequent H4 shift (1,5 H shift) reaction, initiating an additional autoxidation cycle to generate more OOMs. The isomerization reactions involved in the reaction pathways are displayed in Sect. S3 of Supporting Information, and the major products from the reactions of terpinolene with OH/NO_3 are summarized in Sect. S6.

https://doi.org/10.5194/egusphere-2025-3219
Preprint. Discussion started: 25 August 2025

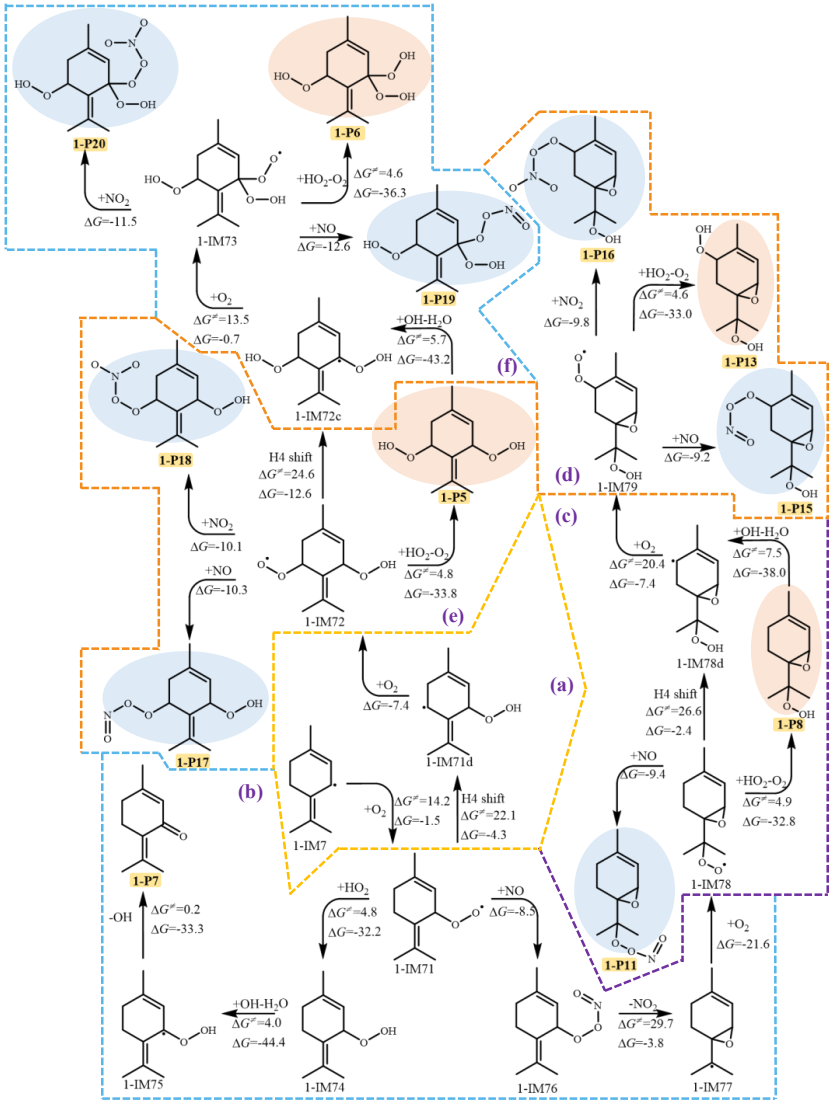

Figure 3. The subsequent reactions of OH-Ter-R• (1-IM7) (unit in kcal mol^{-1}, nitrogen-containing OOMs marked in light blue, nonnitrogenous OOMs marked in lightsalmon)

https://doi.org/10.5194/egusphere-2025-3219
Preprint. Discussion started: 25 August 2025

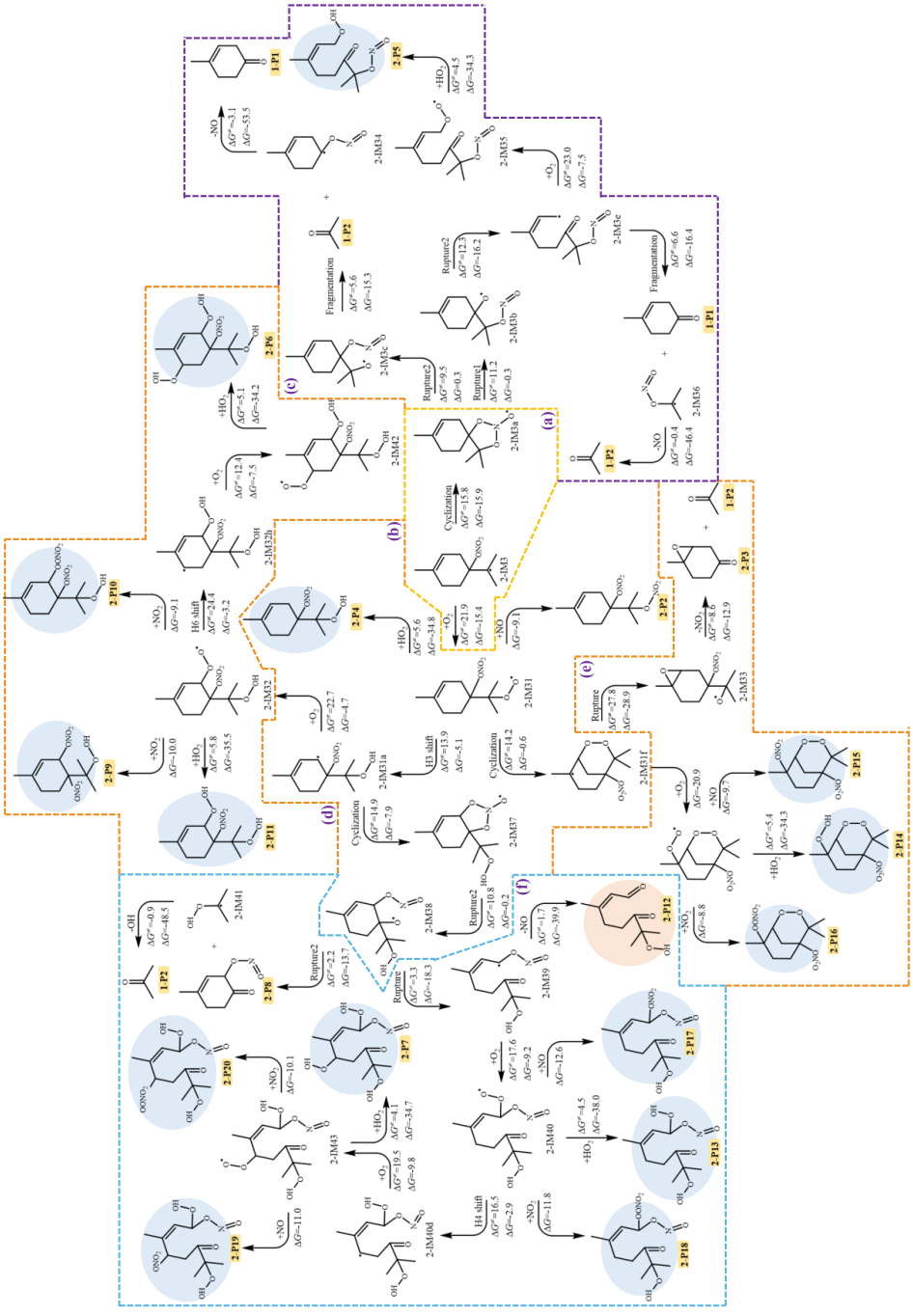

Figure 4. The subsequent reactions of NO_3-Ter-R• (2-IM3) (unit in kcal mol^{-1}, nitrogen-containing OOMs marked in light blue, nonnitrogenous OOMs marked in light salmon)

https://doi.org/10.5194/egusphere-2025-3219
Preprint. Discussion started: 25 August 2025

3.2.2 The atmospheric oxidation of the NO_3-Terpinolene-R• (2-IM3)

The dominant intermediate NO_3-Ter-R• (2-IM3) is prone to cyclization to form a bicyclic alkoxyl radical (2-IM3a), as shown in Fig. 4. Due to the instability of the N-O bond, 2-IM3a undergoes the rupture of O-N bond to produce 2-IM3b or 2-IM3c, which both subsequently proceed with the fragmentation and NO elimination to generate 1-P1 and 1-P2. Besides, Fig. 4(c) indicates that the radical center of 2-IM3b is migrated via C-C bond breaking, and consecutively reacts with O_2 and HO_2 to generate 2-P5. Similar to the intermediate OH-Ter-R• (1-IM4), 2-IM3 also reacts with O_2 to generate the first-generation peroxyl radical (2-IM31), which further reacts with HO_2 to generate 2-P4 (Fig. 4(b)). As the presence of an endocyclic double bond, 2-IM31 proceeds with the cyclization to produce 2-IM31f with a barrier of 14.2 kcal mol^{-1}, followed by O-O bond rupture and NO_2 removal to form 2-P3 and 1-P2, which have been detected in the laboratory studies for the oxidation of terpinolene by NO_3 radical (Fouqueau et al., 2022). Moreover, as shown in Fig. 4(e), the bicyclic alkyl radical 2-IM31f ulteriorly reacts with O_2 to form a new peroxyl radical, resulting in the formation of multiple OOMs.

Among all the H shift reaction pathways (Fig. S11), H3 shift (1,5 H shift) is the dominant reaction pathway to form 2-IM31a, which continues to react with O_2 to produce 2-IM32 or proceed with a cyclization reaction to generate an alkoxy radical 2-IM37. The peroxyl radical 2-IM32 can further undergo the bimolecular reactions with HO_2/NO/NO_2, or continue the autoxidation to produce 2-P6, as shown in Fig. 4(d). For the subsequent reactions of the alkoxy radical 2-IM37, the cleavage of O-N and C-C bond is occurred, followed by OH removal, leading to the formation of 2-P8 and 1-P2. In addition, 2-IM37 can also undergo the rupture of the O-N and C-C bonds to produce the intermediate 2-IM39, which can react with O_2 or eliminate NO to generate a new peroxyl radical 2-IM40 or 2-P12. Subsequently, 2-IM40 proceeds with the autoxidation mechanism driven by H4 shift (1,6-H shift) and then the reaction with HO_2 to generate 2-P7 and 2-P13. The peroxyl radicals (2-IM40 and 2-IM43) can also react with NO/NO_2 to produce nitrogen-containing OOMs, including 2-P17, 2-P18, 2-P19, and 2-P20. According to the field observation of OOMs at a coastal background site in Hong Kong, 2-P6 and 2-P9~2-P20 have been detected (Zheng et al., 2023). Moreover, the MT-mixed-OOMs

https://doi.org/10.5194/egusphere-2025-3219
Preprint. Discussion started: 25 August 2025

identified in the atmospheric monitoring over eastern China's megacities, such as 2-P9, 2-P10, 2-P15 ~ 2-P18, are considered to be generated by the reactions of the peroxyl radicals with NO/NO_2, which is in accordance with the reaction pathways we discussed above (Liu et al., 2023). For clarity, the above-mentioned products that could have been detected in field observations are all summarized in Supplementary Sect. S6.

3.3 Modeling of the yield profiles of OOMs and other main products

Based on the aforementioned oxidation mechanism of terpinolene by OH and NO_3 radical, the thermodynamically feasible reaction pathways were determined, and a zero-dimensional chemical model was further established to calculate the time-dependent fractional yields of the intermediates and major products including OOMs under three atmospheric conditions: (a) in a polluted area (5 ppb NO, 50 ppt HO_2) (Nie et al., 2023; Garmash et al., 2020), (b) in a forested area (50 ppt NO, 50 ppt HO_2), and (c) in a remote area or in the afternoon of an urban area (100 ppt NO, 50 ppt HO_2) (Hofzumahaus et al., 2009; Ma et al., 2021). Based on the bimolecular reaction rate constants of the RO_2 with NO (9.0×10^{-12} cm^3 $molecule^{-1}$ s^{-1}), NO_2 (1.10×10^{-11} cm^3 $molecule^{-1}s^{-1}$) and HO_2 (1.7×10^{-11} cm^3 $molecule^{-1}$ s^{-1}) and the C-centered radicals with O_2 (6.0×10^{-12} cm^3 $molecule^{-1}s^{-1}$) (Wang and Wang, 2016; Wu et al., 2015; Atkinson and Arey, 2003; Boyd et al., 2003; Saunders et al., 2003), the pseudo-first-order rate constants were determined and inputted into the model, as summarized in Supplementary Sect. S4. In the polluted area, the calculated pseudo-first-order rate constant k'_{RO2+NO} (1.21 s^{-1}) is significantly larger than $k'_{RO2+HO2}$ (2.28×10^{-2} s^{-1}). Whereas, under the atmospheric condition of the remote area, where NO concentration is approximately twice of HO_2 concentration, k'_{RO2+NO} (2.42×10^{-2} s^{-1}) and $k'_{RO2+HO2}$ (2.28×10^{-2} s^{-1}) are comparable.

https://doi.org/10.5194/egusphere-2025-3219
Preprint. Discussion started: 25 August 2025

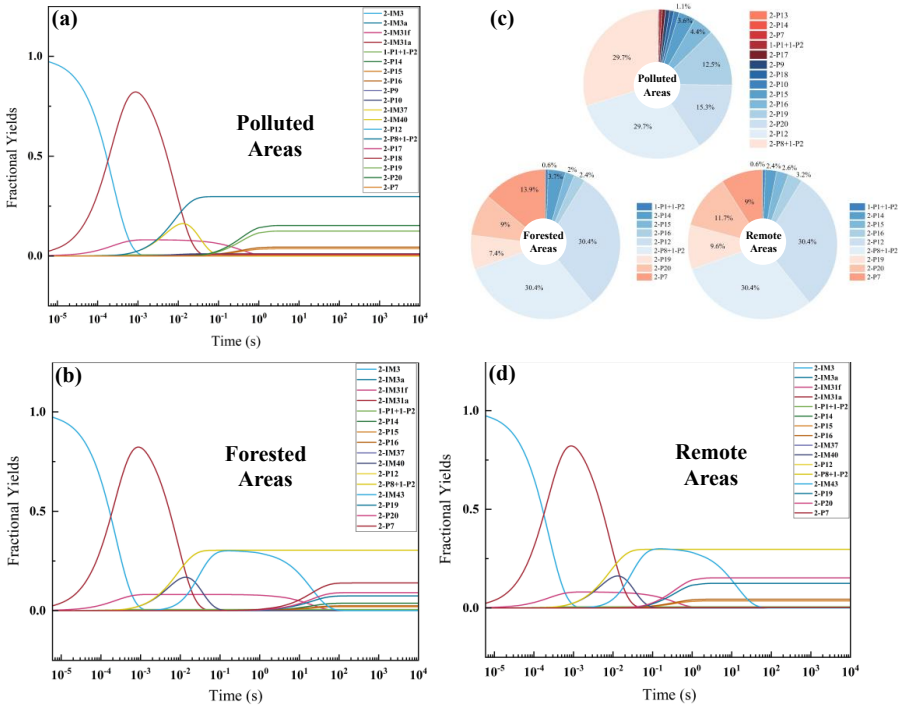

Figure 5. The modeled time-dependent fractional yields of important species generated from the subsequent reactions of NO_3-Ter-R•(2-IM3) under the atmospheric conditions of polluted areas (a), forested areas (b), remote areas (d) (Species with yields <0.1% excluded).

The time-dependent fractional yield of the major products from the oxidation of NO_3-Ter-R• (2-IM3) is shown in Fig. 5. The rate constants of the rate-determining steps for the generation of 2-IM3a, 2-IM31a and 2-IM31f from 2-IM3 were calculated to be 27.1 s^{-1}, 3.83 × 10^3 s^{-1} and 3.42 × 10^2 s^{-1}, respectively. Compared to the bimolecular reaction pathways for the production of 2-P4 and 2-P2, unimolecular reactions are more dominant, among which, 2-IM31a generated by the hydrogen shift reaction is the predominant intermediate. As shown in Fig. 5(a), the fractional yield of 2-IM31a is sharply increased to 91% at ~ 10^{-3} s in the polluted area, accompanied by a rise in the yield of 2-IM31f to ~ 8.0%. Subsequently, the yield of 2-IM31a is declined rapidly to ~ 0%, along with the raising yield of its cyclization product 2-IM37 to ~ 89% at around 10^{-2} s. The continue oxidation of 2-IM37 leads to the increasing yield of 2-IM40, 2-P12, 2-P8 and 1-P2, and then 2-IM43 is generated accompanied by the consumption of 2-IM40 via the autoxidation driven by H4 shift reaction (4.43 × 10 s^{-1}), ultimately, the OOMs 2-P19 and 2-P20 are formed from the reactions of 2-IM43 with NO and NO_2, with their yields

https://doi.org/10.5194/egusphere-2025-3219
Preprint. Discussion started: 25 August 2025

leveled off at 10 s. As indicated in Fig. 5 (b) and (d), the intermediates generated by the unimolecular reactions (such as 2-IM31a, 2-IM43, etc.) are also dominant. Under the polluted atmospheric condition, nitrogen-containing OOMs are generated by the reaction of peroxyl radicals with NO/NO_2, being the predominant pathway, their yields are higher than those in the forest and remote area. Among them, the yields of 2-P19 and 2-P20 are 12.5% and 15.3%, respectively. In the forest and remote area, the reactions of peroxyl radicals with HO_2 can compete with those of peroxyl radicals with NO/NO_2, resulting in an increase in the yield of 2-P7, which is comparable to the yield of 2-P19 and 2-P20. As summarized in Fig. 5 (c), under these three atmospheric conditions, 2-P8, 2-P12, 2-P19, and 2-P20 are the main OOMs with relatively high yields, while 2-P7 is the major OOMs in the forest and remote area (13.9% and 9%, respectively). The total yield of the OOMs (2-P14, 2-P15 and 2-P16) generated by the subsequent oxidation of 2-IM31f produced by the cyclization reaction is approximately 8.0%.

As shown in Fig. S16, in the polluted area, 1-IM42, as the main oxidation product, has a yield as high as 75.4%, followed by 1-P9 (22.8%) and 1-IM43(1.4%). In the forest and remote area, the main oxidation intermediate of 1-IM4 is 1-IM41a generated by the first hydrogen shift reaction, which undergoes bimolecular reactions with HO_2/NO to produce 1-P3 (43.1% and 59.7%), 1-P9 (31.7% and 45.7%), 1-IM42 (3.0 and 5.8%) and 1-IM43 (5.4 and 5.6%). In Fig. S17, in the polluted area, the oxidation product 1-IM76 is dominated with a yield of ~ 95.8%, and the total yield of the remaining products (1-P7, 1-P18 and 1-P17) is approximately ~ 4%. In contrast, under atmospheric conditions in forest and remote areas, the yield of 1-IM76 is declined (31.4% and 47.8%), synchronously, being one of the main oxidation products, the fractional yield of 1-P7 is enhanced to 59.1% and 45%, respectively, with the remaining proportion assigned to 1-P18, 1-P5, and 1-P17. By contrast, there is a significant difference in the yields of OOMs produced from the oxidation of terpinolene by OH and NO_3 radical, mainly due to the different oxidation pathways.

3.4 Volatility distribution of OOMs

The saturation vapor pressures of OOMs can affect their condensation process, which is closely related to SOA formation. Low volatility organic compounds (LVOC) and extremely low volatility organic compounds (ELVOC) have been demonstrated to be a significant

https://doi.org/10.5194/egusphere-2025-3219
Preprint. Discussion started: 25 August 2025

contributor to the growth of a large proportion of the new particles, with a minor contribution from semi-volatile organic compounds (SVOC) (Mohr et al., 2017). Herein, based on the chemical formula and functional groups of the OOMs generated from the oxidation of terpinolene by OH and NO_3, the saturation vapor pressures of the OOMs were firstly predicted using SIMPOL.1 functional group contribution method (Pankow and Asher, 2008; Valorso et al., 2011). It was then converted to the effective saturation concentration (C^*) for further comparison with the estimation by the optimized molecular formula parameterization method (Mohr et al., 2019).

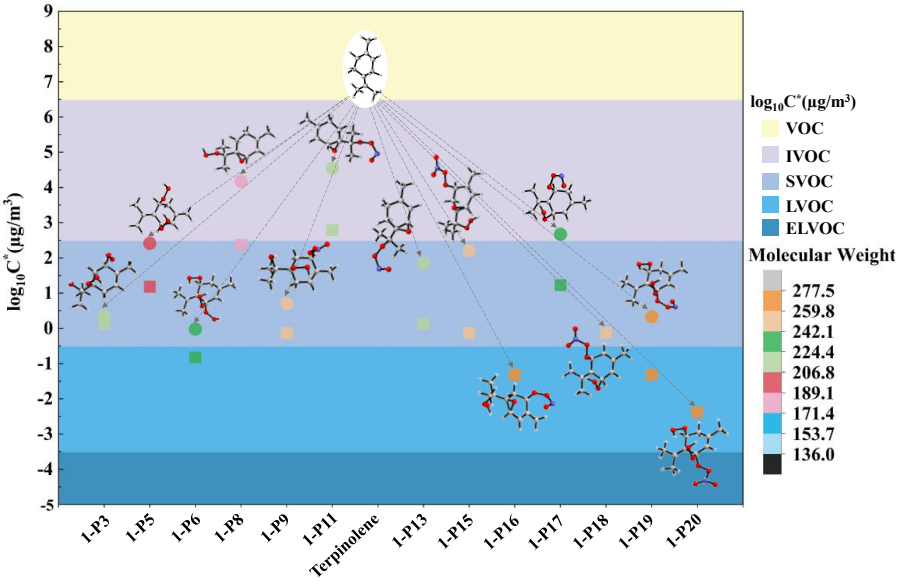

Figure 6. The molecular weight ranges and volatility classifications of C10-OOMs generated from OH-Ter-R•(1-IM4 and 1-IM7) oxidation. (Volatility prediction methods: (○) the functional group contribution method (SIMPOL.1), (□) the molecular formula parameterization method)

As shown in Fig. 6, the OOMs generated from the oxidation of terpinolene with OH are mainly IVOC, SVOC and LVOC. Noteworthily, the results obtained from both methods indicate that most of the OOMs belong to SVOC and LVOC, among which, 1-P6, 1-P16, 1-P19 and 1-P20 are categorized as LVOC by the molecular formula parameterization method, while 1-P6 and 1-P19 are identified as SVOC, according to the functional group contribution method. From the analysis of the atmospheric oxidation mechanism of terpinolene by OH, it can be found that these four OOMs are generated by the subsequent oxidation of the intermediate 1-

https://doi.org/10.5194/egusphere-2025-3219
Preprint. Discussion started: 25 August 2025

IM7 produced by the H-atom abstraction reaction, and the nitrogen-containing OOMs (1-P16, 1-P19, and 1-P20) are produced by the reactions of peroxyl radicals with NO/NO_2. 1-P16 is generated by the reaction of NO_2 with a new peroxyl radical formed by the autoxidation of the peroxyl radical containing a C-O-C ring, which is derived from the reaction of IM7 with NO/O_2. In the previous analysis, we also emphasized the importance of this pathway for the generation of OOMs, due to the existence of $C=C(CH_3)_2$ double bond in the terpinolene molecule, unlike the molecular structures of the products generated from NO_2 elimination in previous studies, a C-O-C ring is formed, leading to the generation of a new alkyl radical, which is conducive to the generation of OOMs.

As revealed in Fig. 7, most of the OOMs generated from the oxidation of terpinolene by NO_3 are nitrogenous OOMs, except for 2-P12. The results obtained from the functional group contribution method indicate that the majority of the nitrogenous OOMs are within the range of SVOC, with only 2-P6, 2-P7 and 2-P19 assigned to LVOC. According to the molecular formula parameterization method, most of the nitrogen-containing OOMs belong to LVOC, with the exception of 2-P19 and 2-P20 sorted as ELVOC. Concretely, 2-P6 is the oxidative product of the adduct 2-IM3 via twice H shifts (1,5- and 1,6-H shift). For the formation of 2-P7, 2-P19 and 2-P20, the alkoxyl radical 2-IM37 undergoes the cleavages of the O-N and C-C bond and the further reaction with O_2 to produce a new peroxyalkyl radical, ultimately producing 2-P7, 2-P19 and 2-P20 through 1,6-H shift, the reaction with NO and NO_2, respectively. Overall, compared to the generated OOMs induced by OH, the effective saturation concentration (C^*) of OOMs derived from the oxidation by NO_3 is generally lower, being more easily distributed into the particle phase. It should be noted that there existed a significant difference in the volatile classification of 2-P14 and 2-P15 containing bicyclic structure utilizing these two methods, even crossing the SVOC range.

https://doi.org/10.5194/egusphere-2025-3219
Preprint. Discussion started: 25 August 2025

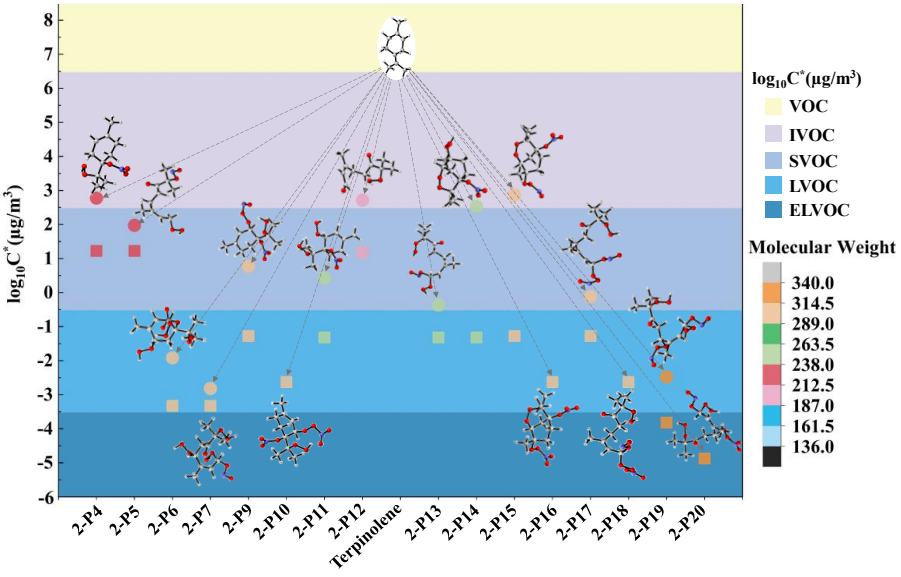

340

341 **Figure 7.** The molecular weight ranges and volatility classifications of C10-OOMs generated
342 from NO_3-Ter-R• (2-IM3) oxidation. (Volatility prediction methods:(○) the functional group
343 contribution method(SIMPOL.1), (□) the molecular formula parameterization method)

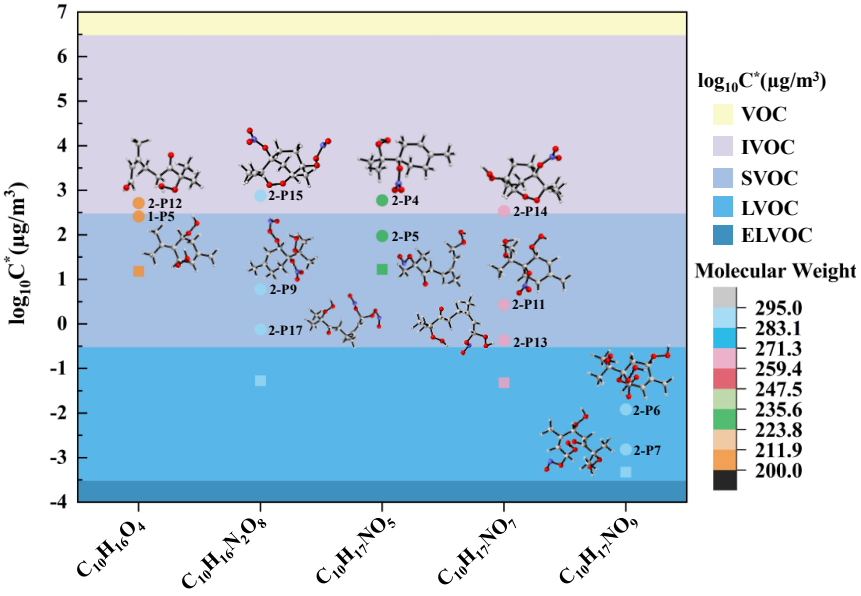

344

345 **Figure 8.** The molecular weight ranges and volatility classifications of C10-OOMs isomers.
346 (Volatility prediction methods: (○) the functional group contribution method(SIMPOL.1), (□)
347 the molecular formula parameterization method)

https://doi.org/10.5194/egusphere-2025-3219
Preprint. Discussion started: 25 August 2025

Based on the molecular structures of each OOMs obtained from quantum chemical calculation, five groups of isomers were emphatically discussed, as shown in Fig. 8, the C^* values of OOMs estimated by the molecular formula parameterization method are generally smaller compared to the results obtained from the functional group contribution method, possibly leading to a distinct underestimation of the saturated vapor pressure, which could affect the accurate assessment of the gas-particle partitioning of OOMs. By contrast, the difference in the effective saturation concentrations of the nitrogen-free OOMs (2-P12 and 1-P5) is small, while those for the other four groups of nitrogen-containing OOMs isomers exist evident differences. Moreover, for the nitrogen-free OOMs (2-P12 and 1-P5), the saturated vapor pressure of 1-P5 with a cyclic structure was relatively lower. For the nitrogen-containing OOMs (the other four groups), the effective saturation concentrations of the isomers in each group follows the rule, i.e., the bicyclic structure > the monocyclic structure > the acyclic structure, which implies that the ring-opening reaction could have an important influence in the generation of the low-volatile products. According to the previous findings of the vital role of isoprene nitrates in new particle formation in upper troposphere over Amazon, the nitrogen-containing OOMs could contribute significantly to SOA formation (Curtius et al., 2024).

4 Conclusion and atmospheric implications

In this work, the atmospheric oxidation mechanism of terpinolene by OH and NO_3 was comprehensively investigated, expounding the formation pathways of OOMs and their molecular structures, indirectly corroborated by the available field observations and laboratory studies. Based on the reaction mechanism, the zero-dimensional chemical model was established to clarify the yield profiles of the main products including OOMs under three typical atmospheric conditions. In addition, the saturation vapor pressures of OOMs were estimated by the SIMPOL.1 method and the molecular formula parameterization method to evaluate their contributions to SOA formation.

We found that the first-generation peroxyl radical (1-IM71), resulting from H-atom abstraction reaction pathway of terpinolene by OH, plays a pivotal role in the formation of C10OOMs. 1-IM71 can undergo twice H shift or the reaction with NO to form a cyclic peroxy radical (1-IM79), ultimately leading to the production of low volatile OOMs (such as 1-P19, 1-

https://doi.org/10.5194/egusphere-2025-3219
Preprint. Discussion started: 25 August 2025

P20 and 1-P16). Among the products, the yields of 1-IM76/1-P7 are accounted for the large proportions (31.4% ~ 95.8%) under three atmospheric conditions. Whereas, the first-generation peroxyl radical formed by OH addition reaction of terpinolene can only proceed with once H shift continued with bond breaking, resulting in the formation of C7OOMs. According to the yield profiles, 1-IM42, 1-P9 and 1-P3 are the main oxidation products with the yields more than 30%. For the oxidation of terpinolene by NO_3, the first-generation peroxyl radical derived from NO_3 addition can also undergo H shift, followed by the cyclization, the rupture of O-N bond and C-C bond, thereby the radical center is migrated, triggering a new round of autoxidation driven by the hydrogen shift reaction to produce nitrogen-containing OOMs, with the yields of 2-P12, 2-P8, 2-P7, 2-P19 and 2-P20 over 10%. Analogously, the adduct generated by NO_3 addition to terpinolene can also produce C10OOMs (2-P5) via cyclization and the cleavage of O-N and C-C bond. Therefore, the reaction pathway of achieving the transfer of the radical center via bond breaking is a new identified but important mechanism for the formation of OOMs except for H shift, which could be applicable to the oxidation of other terpenoids.

The generated OOMs by atmospheric oxidation of terpinolene are mainly IVOC, SVOC, LVOC and some ELVOC, and there is a distinct difference in the effective saturation concentration of the OOM isomers. Compared with the OOMs (mostly I/SVOC) generated from the oxidation of terpinolene by OH radical, the formed nitrogen-containing OOMs (mainly S/LVOC) via the reaction of terpinolene with NO_3 have lower volatility with more potential to contribute to SOA formation. It could be indirectly proved by the measurements in urban atmospheres, the concentrations of nitrogen-containing OOMs dominated the total OOMs during four seasons (Yuan et al. 2024), highlighting its significance in the atmospheric chemistry.

Given multitudinous OOMs formed in the atmosphere, their molecular structures (existing numerous isomers) and formation pathways remain unclear. The findings of this work would be conducive to illuminating the formation mechanism of OOMs by terpene oxidation in the atmosphere and the measurements in the laboratory and field sites. However, it should be noted that the yields of OOMs calculated by the zero-dimensional chemical model could have some uncertainties, derived from the uneven distribution of pollutants, the neglect of advection, diffusion and meteorological factors, incomplete chemical mechanisms, the errors of initial

https://doi.org/10.5194/egusphere-2025-3219
Preprint. Discussion started: 25 August 2025

conditions, time step size and numerical integration, and etc. Therefore, well-integrated models are needed to clarify the coupling of OOMs formation with multiple factors, achieving more accurate predictions.

Code/Data availability

The data and code for quantum chemical calculation and zero-dimensional chemical models used in this study are available upon request.

Supporting Information Available

Detailed information on Fig. S1-S15 and Table S1-S4 are all provided in the supporting information.

Author contributions

JD and HW conceived and designed the study, and wrote the original draft. HW performed the data analysis and created the figures, XZ, WY, ST, and SZ collected the dataset. ST and JD developed the model. SZ, QZ, and WW reviewed and edited the manuscript. All authors participated in the discussion and review of the manuscript.

Competing interests

The contact author has declared that none of the authors has any competing interests.

Acknowledgments

This work was supported by the National Natural Science Foundation of China (No. 22006095, 52106169, 22236004), the China Postdoctoral Science Foundation (No. 2021M690097), and the Future Plan for Young Scholars of Shandong University.

Reference

Arey, J., Atkinson, R., and Aschmann, S. M.: Product Study of the Gas-Phase Reactions of Monoterpenes With the OH Radical in the Presence of NOx, J. Geophys. Res.-Atmos., 95, 18539-18546, 10.1029/JD095iD11p18539, 1990.

Aschmann, S. M., Arey, J., and Atkinson, R.: OH radical formation from the gas-phase reactions of O3 with a series of terpenes, Atmos. Environ., 36, 4347-4355, 10.1016/s1352-2310(02)00355-2, 2002.

Atkinson, R. and Arey, J.: Atmospheric Degradation of Volatile Organic Compounds, Chem. Rev., 103, 4605-4638, 10.1021/cr0206420, 2003.

https://doi.org/10.5194/egusphere-2025-3219
Preprint. Discussion started: 25 August 2025

435 Atkinson, R., Hasegawa, D., and Aschmann, S. M.: Rate Constants for the Gas-Phase Reactions of O3
436 with a Series of Monoterpenes and Related Compounds at 296±2 K, Int. J. Chem. Kinet., 22, 871-887,
437 10.1002/kin.550220807, 1990.
438 Atkinson, R., Aschmann, S. M., Arey, J., and Shorees, B.: Formation of OH Radicals in the Gas Phase
439 Reactions of O3 With a Series of Terpenes, J. Geophys. Res.-Atmos., 97, 6065-6073, 10.1029/92jd00062,
440 1992.
441 Bianchi, F., Garmash, O., He, X. C., Yan, C., Iyer, S., Rosendahl, I., Xu, Z. N., Rissanen, M. P., Riva, M.,
442 Taipale, R., Sarnela, N., Petäjä, T., Worsnop, D. R., Kulmala, M., Ehn, M., and Junninen, H.: The role of
443 highly oxygenated molecules (HOMs) in determining the composition of ambient ions in the boreal forest,
444 Atmos. Chem. Phys., 17, 13819-13831, 10.5194/acp-17-13819-2017, 2017.
445 Bianchi, F., Kurtén, T., Riva, M., Mohr, C., Rissanen, M. P., Roldin, P., Berndt, T., Crounse, J. D.,
446 Wennberg, P. O., Mentel, T. F., Wildt, J., Junninen, H., Jokinen, T., Kulmala, M., Worsnop, D. R.,
447 Thornton, J. A., Donahue, N., Kjaergaard, H. G., and Ehn, M.: Highly Oxygenated Organic Molecules
448 (HOM) from Gas-Phase Autoxidation Involving Peroxy Radicals: A Key Contributor to Atmospheric
449 Aerosol, Chem. Rev., 119, 3472-3509, 10.1021/acs.chemrev.8b00395, 2019.
450 Boyd, A. A., Flaud, P.-M., Daugey, N., and Lesclaux, R.: Rate Constants for RO2 + HO2 Reactions
451 Measured under a Large Excess of HO2, J. Phys. Chem. A, 107, 818-821, 10.1021/jp026581r, 2003.
452 Corchnoy, S. B. and Atkinson, R.: Kinetics of the Gas-Phase Reactions of OH and NO3 Radicals with 2-
453 Carene,1,8-Cineole, p-Cymene, and Terpinolene, Environ. Sci. Technol., 24, 1497-1502,
454 10.1021/es00080a007, 1990.
455 Curtius, J., Heinritzi, M., Beck, L. J., Pöhlker, M. L., Tripathi, N., Krumm, B. E., Holzbeck, P.,
456 Nussbaumer, C. M., Hernández Pardo, L., Klimach, T., Barmpounis, K., Andersen, S. T., Bardakov, R.,
457 Bohn, B., Cecchini, M. A., Chaboureau, J.-P., Dauhut, T., Dienhart, D., Dörich, R., Edtbauer, A., Giez,
458 A., Hartmann, A., Holanda, B. A., Joppe, P., Kaiser, K., Keber, T., Klebach, H., Krüger, O. O., Kürten,
459 A., Mallaun, C., Marno, D., Martinez, M., Monteiro, C., Nelson, C., Ort, L., Raj, S. S., Richter, S.,
460 Ringsdorf, A., Rocha, F., Simon, M., Sreekumar, S., Tsokankunku, A., Unfer, G. R., Valenti, I. D., Wang,
461 N., Zahn, A., Zauner-Wieczorek, M., Albrecht, R. I., Andreae, M. O., Artaxo, P., Crowley, J. N., Fischer,
462 H., Harder, H., Herdies, D. L., Machado, L. A. T., Pöhlker, C., Pöschl, U., Possner, A., Pozzer, A.,
463 Schneider, J., Williams, J., and Lelieveld, J.: Isoprene nitrates drive new particle formation in Amazon's
464 upper troposphere, Nature, 636, 124-130, 10.1038/s41586-024-08192-4, 2024.
465 Draper, D. C., Farmer, D. K., Desyaterik, Y., and Fry, J. L.: A qualitative comparison of secondary organic
466 aerosol yields and composition from ozonolysis of monoterpenes at varying concentrations of NO2,
467 Atmos. Chem. Phys., 15, 12267-12281, 10.5194/acp-15-12267-2015, 2015.
468 Fouqueau, A., Cirtog, M., Cazaunau, M., Pangui, E., Doussin, J. F., and Picquet-Varrault, B.: An
469 experimental study of the reactivity of terpinolene and β-caryophyllene with the nitrate radical, Atmos.
470 Chem. Phys., 22, 6411-6434, 10.5194/acp-22-6411-2022, 2022.
471 Friedman, B. and Farmer, D. K.: SOA and gas phase organic acid yields from the sequential
472 photooxidation of seven monoterpenes, Atmos. Environ., 187, 335-345, 10.1016/j.atmosenv.2018.06.003,
473 2018.
474 Fry, J. L., Draper, D. C., Barsanti, K. C., Smith, J. N., Ortega, J., Winkler, P. M., Lawler, M. J., Brown,
475 S. S., Edwards, P. M., Cohen, R. C., and Lee, L.: Secondary Organic Aerosol Formation and Organic
476 Nitrate Yield from NO3 Oxidation of Biogenic Hydrocarbons, Environ. Sci. Technol., 48, 11944-11953,
477 10.1021/es502204x, 2014.
478 Garmash, O., Rissanen, M. P., Pullinen, I., Schmitt, S., Kausiala, O., Tillmann, R., Zhao, D., Percival, C.,

https://doi.org/10.5194/egusphere-2025-3219
Preprint. Discussion started: 25 August 2025

Bannan, T. J., Priestley, M., Hallquist, Å. M., Kleist, E., Kiendler-Scharr, A., Hallquist, M., Berndt, T., McFiggans, G., Wildt, J., Mentel, T. F., and Ehn, M.: Multi-generation OH oxidation as a source for highly oxygenated organic molecules from aromatics, Atmos. Chem. Phys., 20, 515-537, 10.5194/acp-20-515-2020, 2020.

Griffin, R. J., Cocker, D. R., III, Flagan, R. C., and Seinfeld, J. H.: Organic aerosol formation from the oxidation of biogenic hydrocarbons, J. Geophys. Res. (USA), 104, 3555-3567, 10.1029/1998jd100049, 1999.

Guenther, A. B., Jiang, X., Heald, C. L., Sakulyanontvittaya, T., Duhl, T., Emmons, L. K., and Wang, X.: The Model of Emissions of Gases and Aerosols from Nature version 2.1 (MEGAN2.1): an extended and updated framework for modeling biogenic emissions, Geosci. Model Dev., 5, 1471-1492, 10.5194/gmd-5-1471-2012, 2012.

Guo, Y., Yan, C., Liu, Y., Qiao, X., Zheng, F., Zhang, Y., Zhou, Y., Li, C., Fan, X., Lin, Z., Feng, Z., Zhang, Y., Zheng, P., Tian, L., Nie, W., Wang, Z., Huang, D., Daellenbach, K. R., Yao, L., Dada, L., Bianchi, F., Jiang, J., Liu, Y., Kerminen, V. M., and Kulmala, M.: Seasonal variation in oxygenated organic molecules in urban Beijing and their contribution to secondary organic aerosol, Atmos. Chem. Phys., 22, 10077-10097, 10.5194/acp-22-10077-2022, 2022.

Hakola, H., Arey, J., Aschmann, S. M., and Atkinson, R.: Product formation from the gas-phase reactions of OH radicals and O3 with a series of monoterpenes, J. Atmos. Chem., 18, 75-102, 10.1007/BF00694375, 1994.

Herrmann, F., Winterhalter, R., Moortgat, G. K., and Williams, J.: Hydroxyl radical (OH) yields from the ozonolysis of both double bonds for five monoterpenes, Atmos. Environ., 44, 3458-3464, 10.1016/j.atmosenv.2010.05.011, 2010.

Hofzumahaus, A., Rohrer, F., Lu, K., Bohn, B., Brauers, T., Chang, C.-C., Fuchs, H., Holland, F., Kita, K., Kondo, Y., Li, X., Lou, S., Shao, M., Zeng, L., Wahner, A., and Zhang, Y.: Amplified Trace Gas Removal in the Troposphere, Science, 324, 1702-1704, doi:10.1126/science.1164566, 2009.

Huang, X., Zhou, L., Ding, A., Qi, X., Nie, W., Wang, M., Chi, X., Petäjä, T., Kerminen, V. M., Roldin, P., Rusanen, A., Kulmala, M., and Boy, M.: Comprehensive modelling study on observed new particle formation at the SORPES station in Nanjing, China, Atmos. Chem. Phys., 16, 2477-2492, 10.5194/acp-16-2477-2016, 2016.

Humphrey, W., Dalke, A., and Schulten, K.: VMD: Visual molecular dynamics, J. Mol. Graph., 14, 33-38, https://doi.org/10.1016/0263-7855(96)00018-5, 1996.

Kim, H.: A Density Functional Theory Study on the Reaction Mechanism of Terpinolene with O3, B. Korean Chem. Soc., 37, 121-122, 10.1002/bkcs.10660, 2016.

Kurtén, T., Møller, K. H., Nguyen, T. B., Schwantes, R. H., Misztal, P. K., Su, L., Wennberg, P. O., Fry, J. L., and Kjaergaard, H. G.: Alkoxy Radical Bond Scissions Explain the Anomalously Low Secondary Organic Aerosol and Organonitrate Yields From α-Pinene + NO3, J. Phys. Chem. Lett., 8, 2826-2834, 10.1021/acs.jpclett.7b01038, 2017.

Lee, A., Goldstein, A. H., Keywood, M. D., Gao, S., Varutbangkul, V., Bahreini, R., Ng, N. L., Flagan, R. C., and Seinfeld, J. H.: Gas-phase products and secondary aerosol yields from the ozonolysis of ten different terpenes, J. Geophys. Res.-Atmos., 111, 10.1029/2005jd006437, 2006.

Lindwall, F., Faubert, P., and Rinnan, R.: Diel Variation of Biogenic Volatile Organic Compound Emissions- A field Study in the Sub, Low and High Arctic on the Effect of Temperature and Light, PLOS One, 10, e0123610, 10.1371/journal.pone.0123610, 2015.

Liu, Y., Liu, C., Nie, W., Li, Y., Ge, D., Chen, L., Zhu, C., Wang, L., Zhang, Y., Liu, T., Qi, X., Wang, J.,

https://doi.org/10.5194/egusphere-2025-3219
Preprint. Discussion started: 25 August 2025

Huang, D., Wang, Z., Yan, C., Chi, X., and Ding, A.: Exploring condensable organic vapors and their co-occurrence with PM2.5 and O3 in winter in Eastern China, Environ. Sci. Atmos., 3, 282-297, 10.1039/D2EA00143H, 2023.

Liu, Y., Nie, W., Li, Y., Ge, D., Liu, C., Xu, Z., Chen, L., Wang, T., Wang, L., Sun, P., Qi, X., Wang, J., Xu, Z., Yuan, J., Yan, C., Zhang, Y., Huang, D., Wang, Z., Donahue, N. M., Worsnop, D., Chi, X., Ehn, M., and Ding, A.: Formation of condensable organic vapors from anthropogenic and biogenic volatile organic compounds (VOCs) is strongly perturbed by NOx in eastern China, Atmos. Chem. Phys., 21, 14789-14814, 10.5194/acp-21-14789-2021, 2021.

Lu, T. and Chen, F.: Multiwfn: A multifunctional wavefunction analyzer, J. Comput. Chem., 33, 580-592, https://doi.org/10.1002/jcc.22885, 2012.

Luo, D. M., Pierce, J. A., Malkina, I. L., and Carter, W. P. L.: Rate constants for the reactions of O(3P) with selected monoterpenes, Int. J. Chem. Kinet, 28, 1-8, 10.1002/(sici)1097-4601(1996)28:1<1::Aid-kin1>3.0.Co;2-z, 1996.

Luo, H., Vereecken, L., Shen, H., Kang, S., Pullinen, I., Hallquist, M., Fuchs, H., Wahner, A., Kiendler-Scharr, A., Mentel, T. F., and Zhao, D.: Formation of highly oxygenated organic molecules from the oxidation of limonene by OH radical: significant contribution of H-abstraction pathway, Atmos. Chem. Phys., 23, 7297-7319, 10.5194/acp-23-7297-2023, 2023.

Ma, F., Guo, X., Xia, D., Xie, H.-B., Wang, Y., Elm, J., Chen, J., and Niu, J.: Atmospheric Chemistry of Allylic Radicals from Isoprene: A Successive Cyclization-Driven Autoxidation Mechanism, Environ. Sci. Technol., 55, 4399-4409, 10.1021/acs.est.0c07925, 2021.

Martínez, E., Cabañas, B., Aranda, A., Martín, P., and Salgado, S.: Absolute rate coefficients for the gas-phase reactions of NO3 radical with a series of monoterpenes at T=298 to 433 K, J. Atmos. Chem., 33, 265-282, 10.1023/a:1006178530211, 1999.

Mohr, C., Thornton, J. A., Heitto, A., Lopez-Hilfiker, F. D., Lutz, A., Riipinen, I., Hong, J., Donahue, N. M., Hallquist, M., Petäjä, T., Kulmala, M., and Yli-Juuti, T.: Molecular identification of organic vapors driving atmospheric nanoparticle growth, Nat. Commun., 10, 4442, 10.1038/s41467-019-12473-2, 2019.

Mohr, C., Lopez-Hilfiker, F. D., Yli-Juuti, T., Heitto, A., Lutz, A., Hallquist, M., D'Ambro, E. L., Rissanen, M. P., Hao, L., Schobesberger, S., Kulmala, M., Mauldin III, R. L., Makkonen, U., Sipilä, M., Petäjä, T., and Thornton, J. A.: Ambient observations of dimers from terpene oxidation in the gas phase: Implications for new particle formation and growth, Geophys. Res. Lett., 44, 2958-2966, https://doi.org/10.1002/2017GL072718, 2017.

Nie, W., Yan, C., Huang, D. D., Wang, Z., Liu, Y., Qiao, X., Guo, Y., Tian, L., Zheng, P., Xu, Z., Li, Y., Xu, Z., Qi, X., Sun, P., Wang, J., Zheng, F., Li, X., Yin, R., Dallenbach, K. R., Bianchi, F., Petäjä, T., Zhang, Y., Wang, M., Schervish, M., Wang, S., Qiao, L., Wang, Q., Zhou, M., Wang, H., Yu, C., Yao, D., Guo, H., Ye, P., Lee, S., Li, Y. J., Liu, Y., Chi, X., Kerminen, V.-M., Ehn, M., Donahue, N. M., Wang, T., Huang, C., Kulmala, M., Worsnop, D., Jiang, J., and Ding, A.: Secondary organic aerosol formed by condensing anthropogenic vapours over China's megacities, Nat. Geosci., 15, 255-261, 10.1038/s41561-022-00922-5, 2022.

Nie, W., Yan, C., Yang, L., Roldin, P., Liu, Y., Vogel, A. L., Molteni, U., Stolzenburg, D., Finkenzeller, H., Amorim, A., Bianchi, F., Curtius, J., Dada, L., Draper, D. C., Duplissy, J., Hansel, A., He, X.-C., Hofbauer, V., Jokinen, T., Kim, C., Lehtipalo, K., Nichman, L., Mauldin, R. L., Makhmutov, V., Mentler, B., Mizelli-Ojdanic, A., Petäjä, T., Quéléver, L. L. J., Schallhart, S., Simon, M., Tauber, C., Tomé, A., Volkamer, R., Wagner, A. C., Wagner, R., Wang, M., Ye, P., Li, H., Huang, W., Qi, X., Lou, S., Liu, T., Chi, X., Dommen, J., Baltensperger, U., El Haddad, I., Kirkby, J., Worsnop, D., Kulmala, M., Donahue,

https://doi.org/10.5194/egusphere-2025-3219
Preprint. Discussion started: 25 August 2025

N. M., Ehn, M., and Ding, A.: NO at low concentration can enhance the formation of highly oxygenated biogenic molecules in the atmosphere, Nat. Commun., 14, 3347, 10.1038/s41467-023-39066-4, 2023.
Orlando, J. J., Nozière, B., Tyndall, G. S., Orzechowska, G. E., Paulson, S. E., and Rudich, Y.: Product studies of the OH- and ozone-initiated oxidation of some monoterpenes, J. Geophys. Res.-Atmos., 105, 11561-11572, 10.1029/2000jd900005, 2000.
Orzechowska, G. E.: Atmospheric chemistry of ozone reactions with alkenes, 2003.
Pankow, J. F. and Asher, W. E.: SIMPOL.1: a simple group contribution method for predicting vapor pressures and enthalpies of vaporization of multifunctional organic compounds, Atmos. Chem. Phys., 8, 2773-2796, 10.5194/acp-8-2773-2008, 2008.
Peeters, J., Müller, J.-F., Stavrakou, T., and Nguyen, V. S.: Hydroxyl Radical Recycling in Isoprene Oxidation Driven by Hydrogen Bonding and Hydrogen Tunneling: The Upgraded LIM1 Mechanism, J. Phys. Chem. A, 118, 8625-8643, 10.1021/jp5033146, 2014.
Qiao, X. H., Li, X. X., Yan, C., Sarnela, N., Yin, R. J., Guo, Y. S., Yao, L., Nie, W., Huang, D. D., Wang, Z., Bianchi, F., Liu, Y. C., Donahue, N. M., Kulmala, M., and Jiang, J. K.: Precursor apportionment of atmospheric oxygenated organic molecules using a machine learning method, Environ. Sci. Atmos., 3, 230-237, 10.1039/d2ea00128d, 2023.
Reissell, A., Harry, C., Aschmann, S. M., Atkinson, R., and Arey, J.: Formation of acetone from the OH radical- and O3-initiated reactions of a series of monoterpenes, J. Geophys. Res.-Atmos., 104, 13869-13879, 10.1029/1999jd900198, 1999.
Saunders, S. M., Jenkin, M. E., Derwent, R. G., and Pilling, M. J.: Protocol for the development of the Master Chemical Mechanism, MCM v3 (Part A): tropospheric degradation of non-aromatic volatile organic compounds, Atmos. Chem. Phys., 3, 161-180, 10.5194/acp-3-161-2003, 2003.
Shen, H., Vereecken, L., Kang, S., Pullinen, I., Fuchs, H., Zhao, D., and Mentel, T. F.: Unexpected significance of a minor reaction pathway in daytime formation of biogenic highly oxygenated organic compounds, Sci. Adv., 8, eabp8702, 10.1126/sciadv.abp8702, 2022.
Shu, Y. and Atkinson, R.: Rate constants for the gas-phase reactions of O3 with a series of Terpenes and OH radical formation from the O3 reactions with Sesquiterpenes at 296 ± 2 K, Int. J. Chem. Kinet., 26, 1193-1205, https://doi.org/10.1002/kin.550261207, 1994.
Stewart, D. J., Almabrok, S. H., Lockhart, J. P., Mohamed, O. M., Nutt, D. R., Pfrang, C., and Marston, G.: The kinetics of the gas-phase reactions of selected monoterpenes and cyclo-alkenes with ozone and the NO3 radical, Atmos. Environ., 70, 227-235, https://doi.org/10.1016/j.atmosenv.2013.01.036, 2013.
Surratt, J. D., Gómez-González, Y., Chan, A. W. H., Vermeylen, R., Shahgholi, M., Kleindienst, T. E., Edney, E. O., Offenberg, J. H., Lewandowski, M., Jaoui, M., Maenhaut, W., Claeys, M., Flagan, R. C., and Seinfeld, J. H.: Organosulfate formation in biogenic secondary organic aerosol, J. Phys. Chem. A, 112, 8345-8378, 10.1021/jp802310p, 2008.
Tröstl, J., Chuang, W. K., Gordon, H., Heinritzi, M., Yan, C., Molteni, U., Ahlm, L., Frege, C., Bianchi, F., Wagner, R., Simon, M., Lehtipalo, K., Williamson, C., Craven, J. S., Duplissy, J., Adamov, A., Almeida, J., Bernhammer, A.-K., Breitenlechner, M., Brilke, S., Dias, A., Ehrhart, S., Flagan, R. C., Franchin, A., Fuchs, C., Guida, R., Gysel, M., Hansel, A., Hoyle, C. R., Jokinen, T., Junninen, H., Kangasluoma, J., Keskinen, H., Kim, J., Krapf, M., Kürten, A., Laaksonen, A., Lawler, M., Leiminger, M., Mathot, S., Möhler, O., Nieminen, T., Onnela, A., Petäjä, T., Piel, F. M., Miettinen, P., Rissanen, M. P., Rondo, L., Sarnela, N., Schobesberger, S., Sengupta, K., Sipilä, M., Smith, J. N., Steiner, G., Tomè, A., Virtanen, A., Wagner, A. C., Weingartner, E., Wimmer, D., Winkler, P. M., Ye, P., Carslaw, K. S., Curtius, J., Dommen, J., Kirkby, J., Kulmala, M., Riipinen, I., Worsnop, D. R., Donahue, N. M., and

https://doi.org/10.5194/egusphere-2025-3219
Preprint. Discussion started: 25 August 2025

611 Baltensperger, U.: The role of low-volatility organic compounds in initial particle growth in the
612 atmosphere, Nature, 533, 527-531, 10.1038/nature18271, 2016.
613 Valorso, R., Aumont, B., Camredon, M., Raventos-Duran, T., Mouchel-Vallon, C., Ng, N. L., Seinfeld,
614 J. H., Lee-Taylor, J., and Madronich, S.: Explicit modelling of SOA formation from α-pinene
615 photooxidation: sensitivity to vapour pressure estimation, Atmos. Chem. Phys., 11, 6895-6910,
616 10.5194/acp-11-6895-2011, 2011.
617 Vasudevan-Geetha, V., Tiszenkel, L., Wang, Z., Russo, R., Bryant, D., Lee-Taylor, J., Barsanti, K., and
618 Lee, S. H.: Isomer Molecular Structures and Formation Pathways of Oxygenated Organic Molecules in
619 Newly Formed Biogenic Particles, EGUsphere, 2024, 1-20, 10.5194/egusphere-2024-2454, 2024.
620 Wang, J., Feng, L., Palmer, P. I., Liu, Y., Fang, S., Bösch, H., O'Dell, C. W., Tang, X., Yang, D., Liu, L.,
621 and Xia, C.: Large Chinese land carbon sink estimated from atmospheric carbon dioxide data, Nature,
622 586, 720-723, 10.1038/s41586-020-2849-9, 2020.
623 Wang, S. and Wang, L.: The atmospheric oxidation of dimethyl, diethyl, and diisopropyl ethers. The role
624 of the intramolecular hydrogen shift in peroxy radicals, Phys. Chem. Chem. Phys. (UK), 18, 7707-7714,
625 10.1039/C5CP07199B, 2016.
626 Wang, Y., Clusius, P., Yan, C., Dällenbach, K., Yin, R., Wang, M., He, X.-C., Chu, B., Lu, Y., Dada, L.,
627 Kangasluoma, J., Rantala, P., Deng, C., Lin, Z., Wang, W., Yao, L., Fan, X., Du, W., Cai, J., Heikkinen,
628 L., Tham, Y. J., Zha, Q., Ling, Z., Junninen, H., Petäjä, T., Ge, M., Wang, Y., He, H., Worsnop, D. R.,
629 Kerminen, V.-M., Bianchi, F., Wang, L., Jiang, J., Liu, Y., Boy, M., Ehn, M., Donahue, N. M., and
630 Kulmala, M.: Molecular Composition of Oxygenated Organic Molecules and Their Contributions to
631 Organic Aerosol in Beijing, Environ. Sci. Technol., 56, 770-778, 10.1021/acs.est.1c05191, 2022.
632 Witter, M., Berndt, T., Böge, O., Stratmann, F., and Heintzenberg, J.: Gas-phase ozonolysis:: Rate
633 coefficients for a series of terpenes and rate coefficients and OH yields for 2-methyl-2-butene and 2,3-
634 dimethyl-2-butene, Int. J. Chem. Kinet., 34, 394-403, 10.1002/kin.10063, 2002.
635 Wu, R., Wang, S., and Wang, L.: New Mechanism for the Atmospheric Oxidation of Dimethyl Sulfide.
636 The Importance of Intramolecular Hydrogen Shift in a CH3SCH2OO Radical, J. Phys. Chem. A, 119,
637 112-117, 10.1021/jp511616j, 2015.
638 Zheng, P., Chen, Y., Wang, Z., Liu, Y., Pu, W., Yu, C., Xia, M., Xu, Y., Guo, J., Guo, Y., Tian, L., Qiao,
639 X., Huang, D. D., Yan, C., Nie, W., Worsnop, D. R., Lee, S., and Wang, T.: Molecular Characterization
640 of Oxygenated Organic Molecules and Their Dominating Roles in Particle Growth in Hong Kong,
641 Environ. Sci. Technol., 57, 7764-7776, 10.1021/acs.est.2c09252, 2023.
642 Yuan, Y., Chen, X., Cai, R., Li, X., Li, Y., Yin, R., Li, D., Yan, C., Liu, Y., He, K., Kulmala, M. and Jiang,
643 J.: Resolving Atmospheric Oxygenated Organic Molecules in Urban Beijing Using Online Ultrahigh-
644 Resolution Chemical Ionization Mass Spectrometry. Environ. Sci. Technol., 58(40), 17777-17785,
645 10.1021/acs.est.4c04214, 2024.

https://doi.org/10.5194/egusphere-2025-3219
Preprint. Discussion started: 25 August 2025

646 Graphical Abstract

647

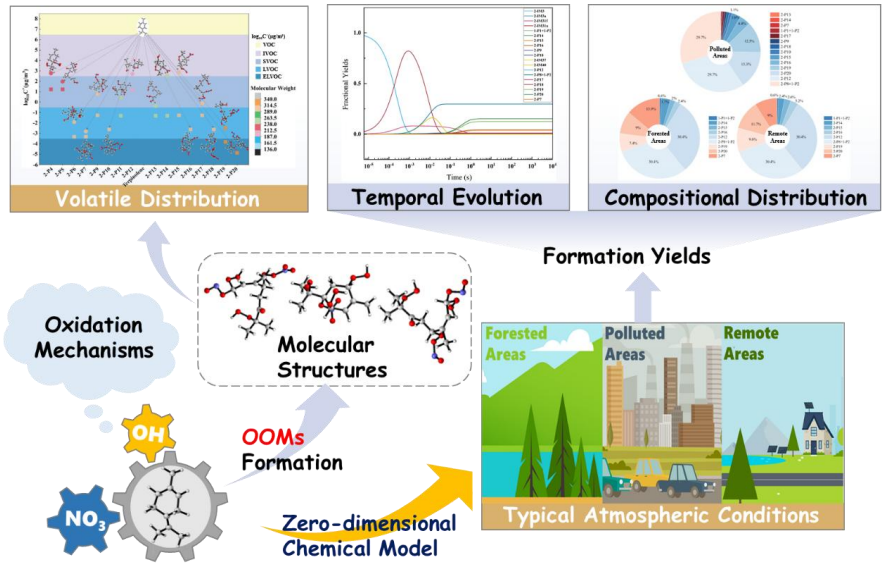

648
649